LAWRENCE
LIVERMORE
NATIONAL
LABORATORY

UCRL-CONF-233640

Cyclic and Linear Polarization of Yttrium-Containing Iron-Based Amorphous Alloys

Sumner D. Day, Tiangan Lian, Joseph C. Farmer, Raul B. Rebak

August 13, 2007

Materials Science and Technology 2007 (MS&T'07)
Detroit, MI, United States
September 16, 2007 through September 20, 2007

Cyclic and Linear Polarization of Yttrium Containing Iron-Based Amorphous Alloys

S. D. Day, T. Lian, J. C. Farmer and Raul B. Rebak
Lawrence Livermore National Laboratory
Livermore, California, USA

Keywords: Iron Amorphous Alloys, Yttrium, Seawater, Corrosion, Ni-Gd, 304B SS

Abstract

Iron-based amorphous alloys are produced by rapid solidification from the melt. These alloys may possess unique mechanical and corrosion resistant properties. The chemical composition of the alloy may influence the cooling rate that is necessary for the alloys to be completely vitreous. At the same time, the corrosion resistance of the amorphous alloys may also depend on their chemical composition. This paper examines the anodic behavior of iron-based amorphous alloys containing three different concentrations (1, 3 and 5 atomic %) of yttrium (Y) in several electrolyte solutions. Results from polarization resistance potentiodynamic polarization show that when the alloy contains 5% atomic Y, the corrosion resistance decreases.

Introduction

Metallic amorphous alloys or metallic glasses have been studied extensively for the last three decades due to their unique characteristics, including superior mechanical properties and corrosion resistance [1]. To produce an amorphous alloy from a liquid state, cooling rates in the order of 10^6 to 1 degrees Kelvin per second are required, depending on the glass forming ability of the melt [1]. The presence of yttrium (Y) in the melt may favor the formation of amorphous alloys. The amorphous alloys are chemically and structurally homogeneous since they do not contain grain boundaries, dislocations and secondary phases, which are common in the crystalline materials [1]. The corrosion resistance of amorphous alloys depends on the alloy composition [2-4]. Amorphous alloys may be more corrosion resistant than their polycrystalline cousins of equivalent composition. Amorphous alloys are hard and can be used in areas where both resistance to wear and corrosion are simultaneously needed. For example the typical Vickers hardness of the polycrystalline Alloy 22 (N06022) is 250 but the Vickers hardness of an amorphous material is higher than 1000 [5]. The fact that amorphous materials are highly corrosion resistant is generally attributed to the absence of crystalline defects in the alloy; however the actual mechanism of this resistance is still not fully understood [1]. When amorphous alloys partially or fully re-crystallize, they may lose some of their characteristic corrosion resistance. This process is called devitrification [6].

The aim of the current study was to study the effect of different amounts of yttrium in the alloy on the corrosion behavior of melt spun ribbons (MSR) in different electrolyte solutions.

Experimental

Table 1 shows the nominal chemical composition of the studied alloys. There were two polycrystalline engineering alloys (borated stainless steel, type 304B or S30466 and the Ni-Gd alloy or N06464) and three amorphous alloys. The borated stainless steel is a typical austenitic stainless steel with the addition of boron and the Ni-Gd alloy is basically the C-4 alloy with the addition of gadolinium, both intended for nuclear applications. The polycrystalline specimens were cut from thick wrought plates in prismatic form (with an connection similar to that described in ASTM G 5) [7]. The area of the 304B SS and the Ni-Gd specimens was 14.4 cm². The amorphous alloys were small ribbons approximately 20 to 50 mm long, 1 mm wide and 25 μm thick (Figure 1). The test area of the ribbons was approximately 0.4 to 1 cm². The ribbons were prepared by dropping molten metal on a water-cooled copper spinning wheel in an inert atmosphere. The initial metal temperature was 1050°C and the wheel was spinning at 17.4 m/sec. The fast cooling fabrication process made the material amorphous. The ribbon had two sides; the side that contacted the spinning wheel was slightly darker and contained small dent-like features and the side that faced away from the wheel was smoother and highly reflective (shiny).

Table 1. Chemical Composition of the Studied Alloys.

Alloy	Approximate Composition A – Weight %, B – Atomic %	Type of Alloy, Specimen
304B SS	Fe-19Cr-14Ni-1.6B [A]	S30466, ASTM A 887
Ni-Gd	Ni-16Cr-15Mo-2Gd [A]	N06464, ASTM B 932
SAM3X1	49.1Fe-19.3Cr-3.1Mo-4.1C-2.9W-1.7Mn-2.9Si-15.8B-1.1Y [B]	Amorphous Melt Spun Ribbon
SAM3X3	49Fe-18.8Cr-3Mo-3.9C-2.8W-1.8Mn-2.2Si-15.5B-3.1Y [B]	Amorphous Melt Spun Ribbon
SAM3X5	48.5Fe-18.3Cr-2.9Mo-3.9C-2.8W-1.2Mn-2.1Si-15.3B-5Y [B]	Amorphous Melt Spun Ribbon

A three-electrode cell (Figure 1), with a capacity of one liter, was used for all the experiments. Generally, 950 mL of electrolyte solution was used in each test. A saturated silver/silver chloride (Ag/AgCl, pre-filled with 4 M KCl saturated with AgCl) reference electrode was used for measuring the potential of the working electrode. The tests were conducted in four electrolyte solutions. Two of these solutions are concentrated versions of ground water at the Yucca Mountain site in Nevada. These multi-ionic solutions are called simulated concentrated water (SCW) and simulated acidified water (SAW) (Table 2). SCW has an alkaline pH of approximately 8 and is the solution that results by concentrating the ground water by a factor of 1000 (via the evaporation of water). The SAW solution has a pH of approximately 3 and is an acidified version of SCW to simulate the activity of microorganisms and the acidification that may result by the hydrolysis of metallic corrosion products. The bridge in the electrochemical cell between the reference electrode and the Luggin capillary was also filled with the test solution of interest. A water cooled jacket was used to maintain the reference electrode at near room temperature. A platinum (Pt) sheet welded to a Pt wire was used as a counter electrode. The electrochemical cell was heated using a heating mantle. Nitrogen gas was bubbled through the test solution for deaeration. The gas exited the cell though a condenser and a liquid trap to prevent evaporation of the solution and the ingress of air into the test cell. The deaeration was started 24 hour before the electrochemical tests. During this period the evolution

of the corrosion potential was monitored. The electrochemical polarization measurements were conducted through a commercial potentiostat that was integrated with a desktop computer and the companion software.

Table 2. Chemical Composition of the Multi-ionic Solutions (mg/L).

	K^+	Na^+	Mg^{2+}	Ca^{2+}	F^-	Cl^-	NO_3^-	SO_4^{2-}	HCO_3^-	SiO_2^-	pH
SCW	3,400	40,900	<1	<1	1,400	6,700	6,400	16,700	70,000	27	7.9
SAW	3,400	37,690	1,000	1,000	0	24,250	23,000	38,600	0	27	2.7

The electrochemical test sequence consisted of three steps; (1) Monitoring the corrosion potential for 24 h, (2) Three consecutive polarization resistance tests (ASTM G 59 and G 102) [7], and (3) A cyclic potentiodynamic polarization (CPP) (ASTM G 61) [7] test. For the polarization resistance and the CPP polarization tests, a potential scan rate of 600 mV per hour (0.167 mV/s) was used. In the polarization resistance tests the potential was scanned from 20 mV below the instantaneous corrosion potential to 20 mV above the corrosion potential. This test lasts approximately 3 minutes. For the CPP tests the scan was started at 100 mV below the instantaneous corrosion potential and the scan was reversed when the current density reached 5 mA/cm² or 1.2 V. From the CPP tests several parameters can be obtained. These parameters are grouped into (1) Breakdown potentials (E20 and E200, which are the potentials in the forward scan that need to be reached to obtain current densities of 20 and 200 μA/cm² respectively) and (2) Repassivation potentials (ER10, ER1 and ERCO). ER10 and ER1 are the potentials in the reverse scan that need to be reached to obtain current densities of 10 and 1 μA/cm². ERCO is the potential at which the reverse scan crosses over (CO) the forward scan.

The corrosion rate was estimated from the polarization resistance tests using the following formulas given in ASTM standards G 59 and G 102 [7]

$$i_{corr} = \frac{1}{R_p} \times \frac{b_a \cdot b_c}{2.303(b_a + b_c)}$$

$$CR(\mu m / yr) = k \frac{i_{corr}}{\rho} EW$$

where k is a constant (3.27 x 10^{-3} mm g/μA cm yr). The Tafel constants b_a and b_c were assumed to be ± 120 mV/decade. The values of density (ρ) and equivalent weight (EW) used for the calculations of corrosion rates are given in Table 3.

Table 3. Used values of density and equivalent weight.

	Density (g/cm³)	Equivalent Weight (dimensionless)
SAM3X	8	26
304B	7.9	25.12
Ni-Gd	8.76	27.09

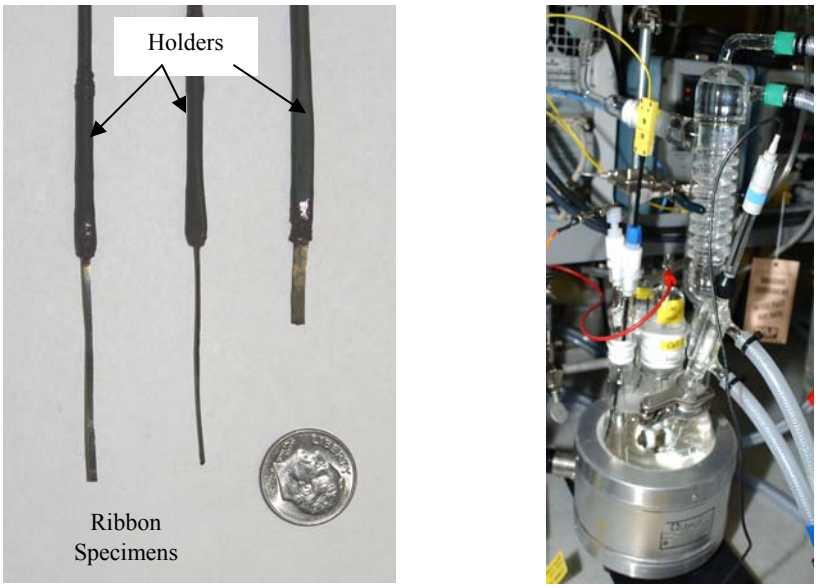

Figure 1. Ribbon Specimens and Testing Cell

Results

Corrosion Potential and Corrosion Rate of Ribbons

Figure 2 and Table 4 show the values of the corrosion potential (E_{corr}) for the melt spun ribbons (MSR) after 24-hr immersion in the four tested electrolyte solutions. These E_{corr} values are for short immersion times in deaerated solutions and therefore they are not intended to represent the behavior of the alloys after long immersion times in aerated solutions. Nevertheless, the 24-hr E_{corr} of the three alloys in the pure salt solutions (3.5 m NaCl and 5 M $CaCl_2$) shows that as the amount of yttrium in the ribbon increased the E_{corr} decreased, suggesting that the alloy became more active for increased yttrium concentrations. Figure 2 also shows that the E_{corr} in the NaCl solution was slightly lower than in the $CaCl_2$ probably because the pH of the NaCl solution was probably one unit higher than the pH in the $CaCl_2$ solution.

For the ribbons immersed in the SAW solution, the 24-hr E_{corr} increased as the content of yttrium in the alloy increased. The SAW solution is acidic and generally oxidizing, therefore the E_{corr} values of the alloys tend to be higher. Estill et al. reported that the long-term E_{corr} of Alloy 22 in SAW solution was approximately +400 mV SSC [8]. The 24-hr E_{corr} in the SCW solution was not a simple function of the content of yttrium since it seemed to decrease for the 3%Y content and later increase for the 5%Y content.

Table 4 also shows the average corrosion rate (CR) for the ribbons with the three yttrium contents. As stated above, the corrosion rate was calculated using the polarization resistance test (ASTM G 59). Three consecutive tests were performed for each specimen in Table 2. The fitting of the data to calculate R_p was carried out using a ±10 mV potential range with respect to the instantaneous corrosion potential. The average value of the corrosion for three measurements is reported in Table 4. These corrosion rates are for a 24-hr immersion time in deaerated solutions and they are not intended to represent the long-term behavior of these alloys in aerated

environments. Figure 3 shows the average corrosion rates of the tee type of ribbons in the two chloride solutions (NaCl and $CaCl_2$). The average CR increased as the amount of yttrium increased in the alloy. This behavior corresponded well with the decrease in the E_{corr} as the yttrium content increased (Figure 2) showing that the ribbons became more active with an increase in yttrium.

The CR in the multi-ionic solutions (SAW and SCW) was not as well defined as in the pure chloride solutions. The reason for this is because the SAW and SCW solutions are less aggressive and therefore the values of CR are less reproducible. Moreover, the tests shown in Table 4 are for a single specimen in each condition. If at least three specimens are tested in each condition, a more accurate statistical analysis can be made.

Table 4. Experimental Results in Seawater at 90°C

Specimen	Electrolyte	Test Temp. (°C)	E_{corr} 24-hr.	Average CR (μm/year)	E20 mV SSC	E200 mV SSC	ER10 mV SSC	ER1 mV SSC	ERCO mV SSC
SAM3X1R1	SAW	90	-380	1.272	740	1031	799	656	880
SAM3X3R2	SAW	90	217	0.091	707	1010	663	532	822
SAM3X5R3	SAW	90	309	0.113	704	995	666	505	799
BS01	SAW	90	-317	4.126	5	17	-170	-211	-210
NG01	SAW	90	-348	38.310	668	698	538	-20	468
SAM3X1R2	SCW	90	-173	0.051	823	871	629	491	552
SAM3X3R3	SCW	90	-531	5.167	732	832	194	99	409
SAM3X5R4	SCW	90	-191	0.093	783	846	230	169	510
BS02	SCW	90	-425	0.447	218	793	321	141	757
NG02	SCW	90	-417	0.419	673	700	590	583	589
SAM3X1R5	3.5m NaCl	90	-103	0.021	984	1043	859	769	784
SAM3X3R1	3.5m NaCl	90	-450	0.062	934	993	822	655	703
SAM3X5R1	3.5m NaCl	90	-444	0.620	933	986	199	-187	-208
BS04	3.5m NaCl	90	-578	1.840	-219	-203	-480	-563	
NG04	3.5m NaCl	90	-539	8.114	-322	-281	-317	-363	-8
SAM3X1R3	5 M $CaCl_2$	105	38	0.022	962	996	744	661	690
SAM3X3R4	5 M $CaCl_2$	105	-251	0.056	777	842	693	565	546
SAM3X5R2	5 M $CaCl_2$	105	-310	0.096	-32	-2	<-288	<-288	
BS03	5 M $CaCl_2$	105	-352	2.540	-273	-268			
NG03	5 M $CaCl_2$	105	-419	52.703	-371	-320	-339	-370	-135

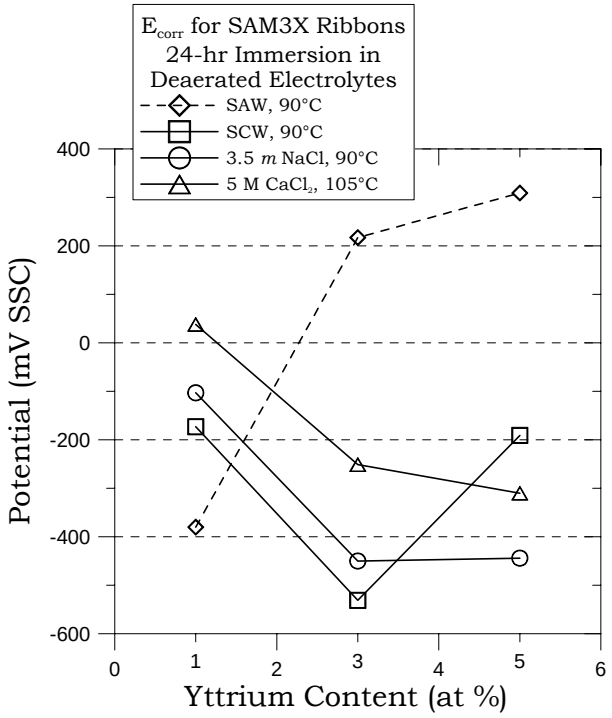

Figure 2. 24-hr corrosion potential as a function of yttrium content

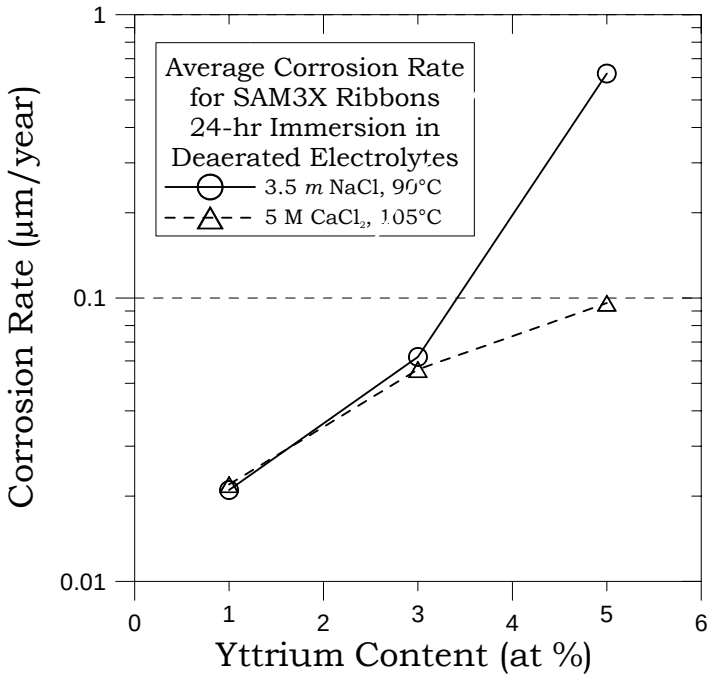

Figure 3. Corrosion rate in chloride solutions as a function of yttrium content)

Cyclic Potentiodynamic Polarization (CPP) tests

Figure 4 and 5 show the cyclic potentiodynamic polarization (CPP) curves of the three ribbons in SAW and 3.5 m NaCl solutions, respectively. For the SAW solution only the forward part of the test is shown for clarity purposes (Figure 4). Figure 4 shows that as the yttrium content in the alloy increased the corrosion potential (E_{corr}) increased and the initial passive current density decreased. However, above 600 mV SCC (at potentials near the breakdown potential) the polarization curves for the three ribbons looked exactly the same. None of these ribbons suffered localized corrosion attack during the tests. Figure 5 shows that as the amount of yttrium in the alloys increased the corrosion potential slightly decreased and the passive current density in the forward scan increased. This plot shows again that the increase in the yttrium content in the alloy made it more active (less passive) when tested in the NaCl solution. Figure 5 also shows that the repassivation potential decreased as the yttrium content increased.

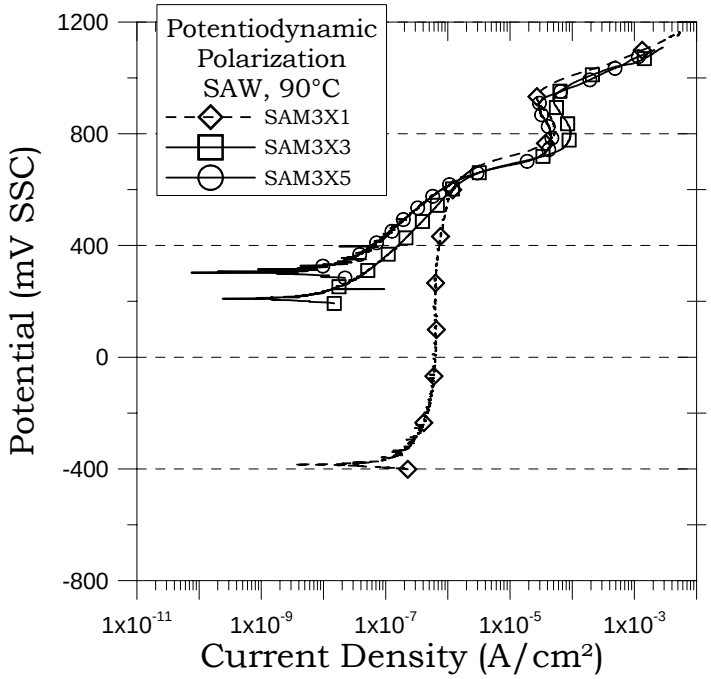

Figure 4. Cyclic potentiodynamic polarization ribbons with different yttrium content in SAW at 90°C.

Parameters from the CPP tests

Instead or plotting all the polarization curves for the tests listed in Table 4, it is useful to only use specific points from the curves. In Table 4, E20 and E200 represent values of breakdown potential. They are the values of potential for which the current density in the forward scan is 20 and 200 μA/cm². Similarly, ER10, ER1 and ERCO are values of repassivation potential. ER10 and ER1 represent values of potential in the reverse scan for which the current density is respectively 10 and 1 μA/cm². ERCO is the potential at which the reverse scan crosses over (CO) the forward scan. Table 4 lists all the parameters from the CPP for all the tested

specimens. Figure 6 shows the breakdown potential E20 as a function of the yttrium content for four tested solutions. For the two multi-ionic solutions (SAW and SCW) and for the NaCl solutions the E20 only slightly decreased as the amount of yttrium in the alloy increased. However, the values of E20 were high (above 600 mV) showing that these alloys were resistant to passivity breakdown under the tested conditions. In the 5 M $CaCl_2$ solution, the E20 decreased approximately 1 V as the amount of yttrium in the alloys increased from 1% to 5%.

Figure 7 shows the repassivation potential ER1 as a function of the yttrium content in the alloy in the four tested solutions. For all the tested solutions, as the amount of yttrium increased the repassivation potential decreased, suggesting that the alloys became more susceptible to localized corrosion at the higher yttrium contents. The most significant decrease was for the tests in the pure chloride solutions (NaCl and $CaCl_2$) where the decrease in ER1 was approximately 800 mV. The least amount of decrease in ER1 was in the SAW solution suggesting that even the 5%Y content alloy was resistant to localized corrosion in this environment.

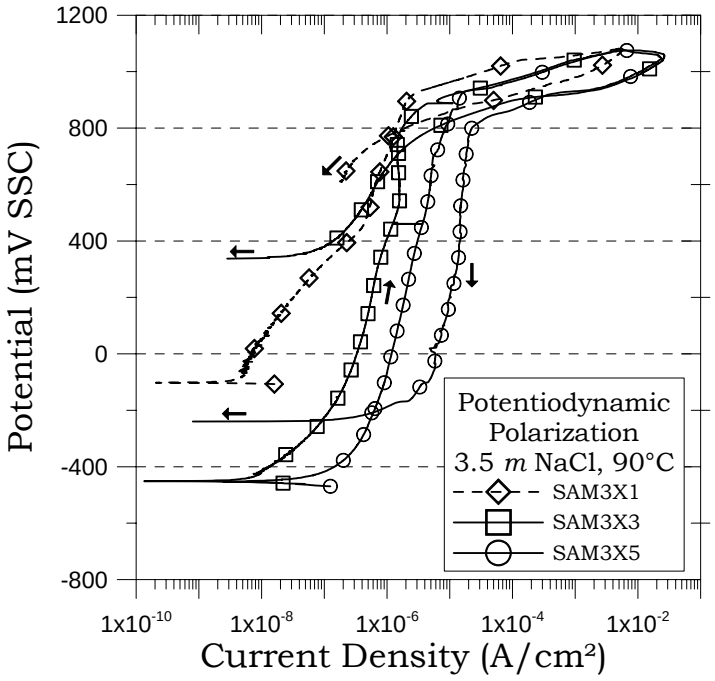

Figure 5. Cyclic potentiodynamic polarization ribbons with different yttrium content in 3.5 m NaCl at 90°C

Comparative Behavior between Amorphous and Polycrystalline Alloys

Figure 8 shows the cyclic potentiodynamic polarization in SAW at 90°C of the ribbon containing the intermediate amount of yttrium (3 at%) compared to the behavior of two commercial alloys for similar intended applications (304B SS and Ni-Gd alloy). The 304B SS alloy had a low passive current density of approximately 1 μA/cm² but a low breakdown potential of near 0 V (see also Table 4). The reverse scan showed significant amount of hysteresis suggesting the presence of localized corrosion. The Ni-Gd alloy had a higher passive current density than the 304B SS but also had a longer passive region of potentials of

approximately 800 mV (Figure 8). The reverse scan of the Ni-Gd alloy showed little or no hysteresis suggesting a resistance to localized corrosion. The lowest passive current density was for the amorphous SAM3X3 ribbon (Figure 8). Also, the reverse scan for the SAM3X3 alloy showed little or no hysteresis even though the alloy was polarized to higher potentials than the other two alloys (up to approximately 1.2 V SSC).

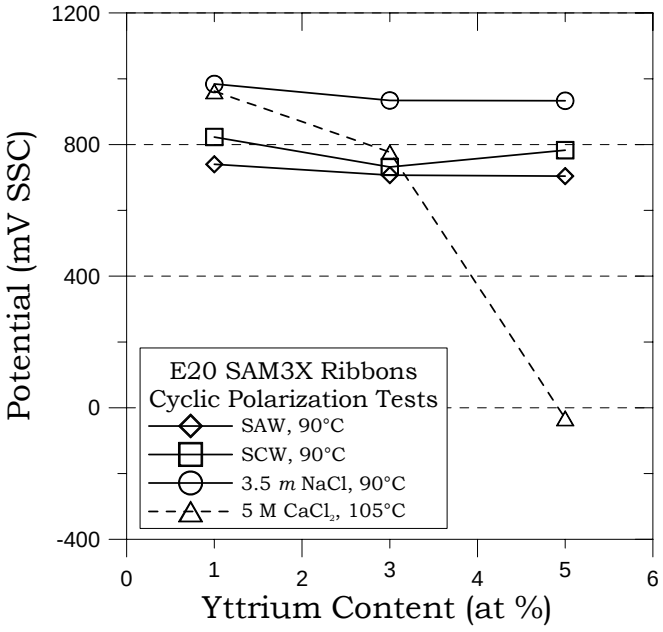

Figure 6. Breakdown potential E20 as a function of yttrium content

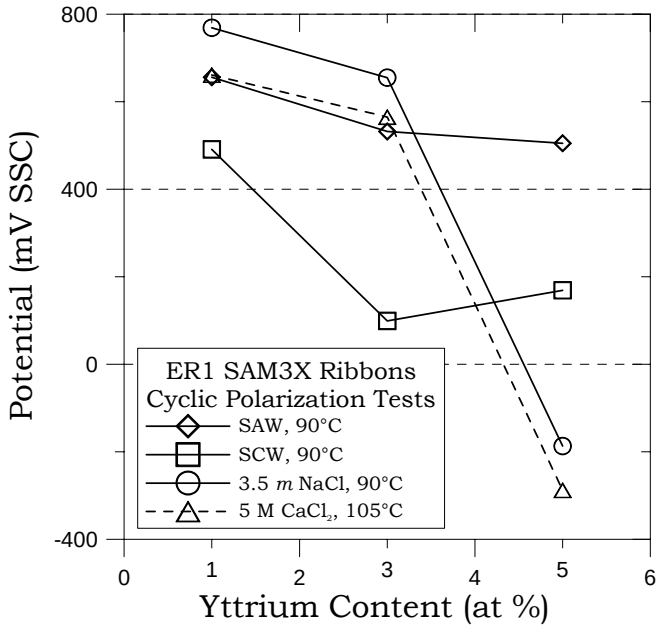

Figure 7. Repassivation potential ER1 as a function of yttrium content

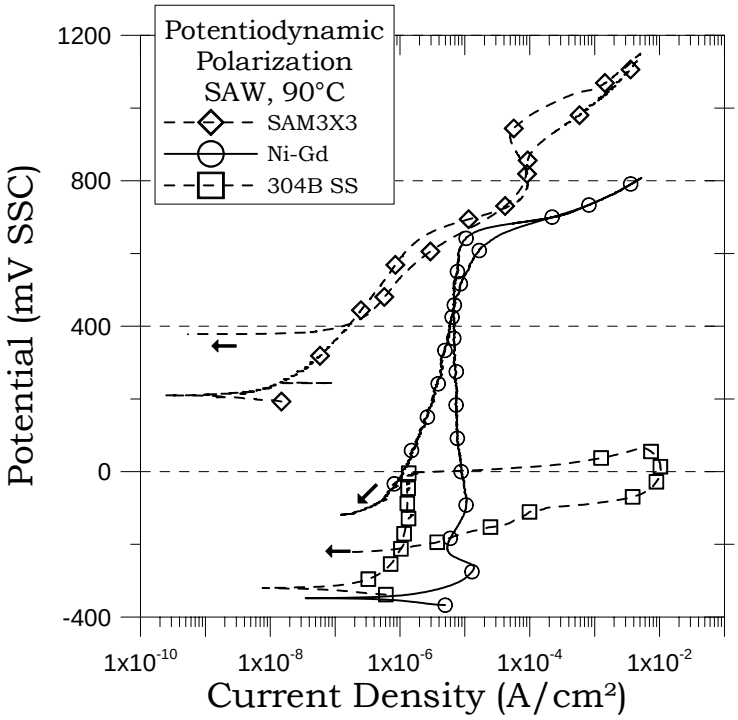

Figure 8. Comparison on the anodic behavior of SAM3X3, 304B SS and Ni-Gd Alloys in SAW at 90°C

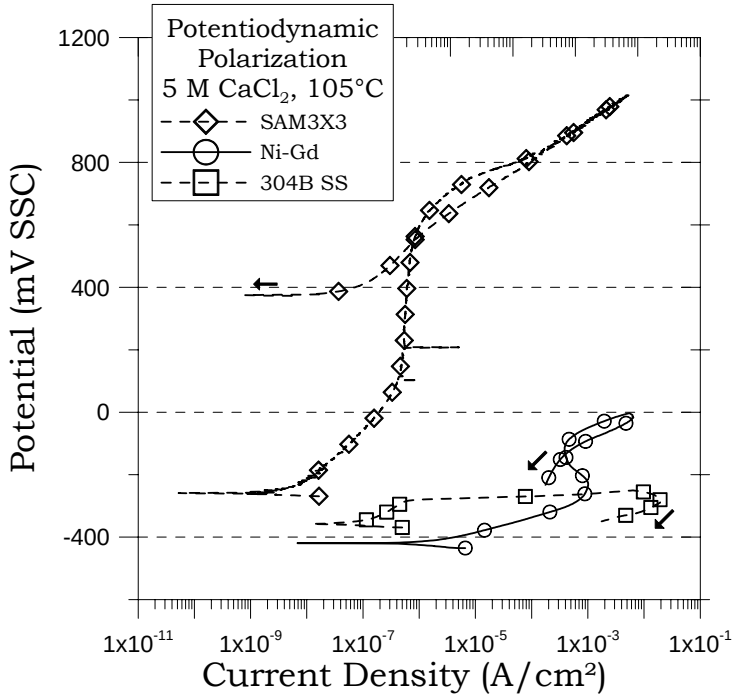

Figure 9. Comparison on the anodic behavior of SAM3X3, 304B SS and Ni-Gd Alloys in 5 M $CaCl_2$ at 105°C

Figure 9 shows comparatively the behavior of SAM3X3 with 304B SS and Ni-Gd alloy. For both the stainless steel and the Ni-Gd alloy, the passive region was small or non-existent and the breakdown and repassivation potentials were low (less than –200 mV SSC) showing little resistance of these alloys to localized corrosion in 5 M $CaCl_2$ at 105°C [9]. On the other hand the passive current density for the amorphous ribbon was lower than 1 μA/cm² and the breakdown and repassivation potentials were higher than 500 mV SSC.

Summary and Conclusions

- The addition of 1 and 3% yttrium to the amorphous ribbon does not affect the corrosion resistance in hot concentrated chloride solutions of the melt spun ribbons
- The addition of 5% Y results in a decreased resistance to corrosion of the ribbons in similar electrolytes.
- For hot concentrated ground water type solutions, the effect of yttrium addition was not detrimental.
- The resistance to localized corrosion of amorphous ribbons (especially the ones containing 1% and 3% Y) are much more resistant to general and localized corrosion than other commercial alloys such as 304B SS and Ni-Gd alloy.

Acknowledgements

This work was performed under the auspices of the U. S. Department of Energy by the University of California Lawrence Livermore National Laboratory under contract W-7405-Eng-48. Work was sponsored by the United States Department of Energy (DOE), Office of Civilian Radioactive Waste Management (OCRWM) and the Defense Advanced Research Projects Agency (DARPA), Defense Science Office (DSO). The guidance of Leo Christodoulou at DARPA DSO and of Jeffrey Walker at DOE OCRWM is gratefully acknowledged.

Disclaimer

References

1. J. R. Scully and A. Lucente, "Corrosion of Amorphous Metals," ASM Handbook, Volume 13B, Corrosion: Materials, p. 476 (ASM International, 2005: Materials Park, OH).
2. K. Hashimoto, K. Asami, M. Naka and T. Masumoto, Corr. Sci., 19, 857 (1979)
3. K. Asami, M. Naka, K. Hashimoto and T. Masumoto, J. Electrochem. Soc., 127, 76 (1991).
4. H. Habazaki, A. Kawashima, K. Asami and K. Hashimoto, J. Electrochem. Soc., 138, 2130 (1980).
5. R. B. Rebak, L. F. Aprigliano, S. D. Day, and J. C. Farmer, "Salt Fog Testing of Iron-Based Amorphous Alloys," Paper NN3.14, in proceedings of the symposium Scientific Basis for Nuclear Waste Management XXX in the Materials Research Society annual conference, 28 November to 01 December 2006, Boston MA.
6. J. R. Scully, A. Gebert and J. H. Payer, *Journal of Materials Research*, **22**, 302 (2007).
7. ASTM International, Volume 03.02, Corrosion of Metals, (ASTM International, 2004: West Conshohocken, PA).
8. J. C. Estill, G. A. Hust and R. B. Rebak, "Long Term Corrosion Potential Behavior of Alloy 22 in Yucca Mountain Relevant Environments," Paper 03688 in Corrosion/2003 Conference (Houston, TX: NACE International, 2003)
9. R. B. Rebak, S. D. Day, T. Lian, L. F. Aprigliano, P. D. Hailey and J. C. Farmer, "Enhanced Corrosion Resistance of Iron-Based Amorphous Alloys," in proceedings of the PVP-ASME conference, 22-26 July 2007 (San Antonio, TX).